Journal of Advanced Ceramics
2013, 2(2): 112–118
DOI: 10.1007/s40145-013-0048-y ISSN 2226-4108

Research Article

Electrical properties of $Na_2Pb_2R_2W_2Ti_4V_4O_{30}$ (R = Dy, Pr) ceramics

Piyush R. DAS*, B. N. PARIDA, R. PADHEE, R. N. P. CHOUDHARY

Department of Physics, *Institute of Technical Education & Research*, *Siksha 'O' Anusandahan University*, *Khandagiri*, *Bhubaneswar 751030*, *Odisha*, *India*

Received: January 11, 2013; Revised: February 06, 2013; Accepted: February 16, 2013

Abstract: The polycrystalline samples of complex tungsten bronze (TB) $Na_2Pb_2R_2W_2Ti_4V_4O_{30}$ (R=Dy, Pr) compounds were prepared by solid-state reaction technique. Room- temperature preliminary structural studies confirm the formation of the compounds in the orthorhombic crystal system. Detailed studies of electrical properties of the materials using complex impedance spectroscopy technique exhibit that the impedance and related parameters are strongly dependent upon temperature and microstructure (bulk, grain boundary, etc). An observation of negative temperature coefficient of resistance (NTCR) suggests the materials have semiconducting properties. The variation of AC conductivity with temperature shows a typical Arrhenius behavior of the materials. Both the samples obey Jonscher's universal power law. The existence of hopping mechanism in the electrical transport processes in the system with non-exponential type of conductivity relaxation is confirmed by electrical modulus analysis.

Keywords: ceramics; impedance spectroscopy; electrical properties; ferroelectricity; microstructure

1 Introduction

Though a large number of ferroelectric oxides of different structural family are known today, some ferroelectrics with tungsten bronze (TB) structure have fascinated many researchers because of their interesting physical properties useful for transducer, multi-layered capacitors, microwave dielectric resonators, pyroelectric detectors, actuators, etc. The TB structure has complex crystal structure with a general chemical formula $[(A_1)_2(A_2)_4(C)_4][(B_1)_2(B_2)_8]O_{30}$, where the A-sites are usually filled by mono-trivalent cations, and the B-sites by W^{6+}, Ti^{4+}, Nb^{5+}, Ta^{5+} or V^{5+} atoms. As the C-site is generally empty, the above formula reduces to $A_6B_{10}O_{30}$. The physical properties of the materials with the TB structure can thus be tailored by the substitution of varieties of cations at different interstitial sites for various applications. Detailed literature survey on various physical properties of TB structure reveals that a lot of work has been done in the past on ferroelectric ceramics of this family [1–10]. The structure and ferroelectric properties in six-valence complex TB structure compounds such as $Na_2Pb_2Sm_2W_2Ti_4Nb_4O_{30}$ [11], $Na_2Pb_2Nd_2W_2Ti_4Nb_4O_{30}$ [12], and $Na_2Pb_2R_2W_2Ti_4V_4O_{30}$ (R = Gd, Eu) [13] have already been reported by us. We have already reported the details of thermo-gravimetry analysis (TGA), crystal structure at room temperature, microstructure, ferroelectric properties and AC conductivity of the titled compounds: $Na_2Pb_2Dy_2W_2Ti_4V_4O_{30}$ (NPDWTV) and $Na_2Pb_2Pr_2W_2Ti_4V_4O_{30}$ (NPPWTV) [14]. In the present work, we mainly report the impedance properties of these materials.

* Corresponding author.
E-mail: prdas63@gmail.com

2 Experiment

The polycrystalline samples of $Na_2Pb_2Dy_2W_2Ti_4V_4O_{30}$ and $Na_2Pb_2Pr_2W_2Ti_4V_4O_{30}$ were prepared relatively at low temperature using a standard mixed-oxide method with high-purity raw materials (analytical reagent grade): Na_2CO_3, PbO, Dy_2O_3, Pr_2O_3, TiO_2, V_2O_5 and WO_3. These oxides and carbonate were thoroughly mixed in dry (air) and wet (methanol) medium each for 1 h using agate mortar. The calcination temperature was optimized using TGA and repeated firing. Finally, the physical mixtures were calcined at 650 ℃ for 4 h in alumina crucibles. The formation of compounds was checked by X-ray diffraction (XRD) technique using X-ray powder diffractometer (Rigaku Miniflex, Japan, Cu Kα radiation). The calcined powders were pelletized and sintered at 675 ℃ for 4 h. The pellets were coated with high-quality silver paste and dried at 150 ℃. The impedance and related parameters were measured on the pellets using a computer-controlled Hioki-LCR Hi-TESTER (Model 3532, Japan) as a function of frequency (100 Hz–1 MHz) at different temperatures (25–500 ℃).

3 Results and discussion

3.1 Sample preparation and XRD analysis

The samples of NPDWTV and NPPWTV were prepared relatively at low temperature using a standard mixed-oxide method. In our previous work [14], the diffraction peaks of the ceramics are indexed using the standard computer program POWD [15] and the orthorhombic crystal structure is selected. The least-square lattice parameters (as reported) are: a = 18.8696(12) Å, b = 19.8915(12) Å, c = 3.8018(12) Å for NPDWTV, and a = 19.7863(7) Å, b = 19.9355(7) Å, c = 3.7269(7) Å for NPPWTV (estimated standard deviation in parenthesis).

3.2 Complex impedance analysis

Complex impedance spectroscopy (CIS) is a non-destructive and powerful technique to study the electrical properties of ferroelectrics and ionic conductors over a wide range of frequency and temperature. This technique also enables us to estimate the contribution of bulk, grain boundary and material electrode polarization in the impedance. For this, AC signal is applied across the sample and the output response is then measured. The impedance and related parameters of the materials give us both real (resistive) and imaginary (reactive) components. The AC response of a material is generally expressed as follows:

complex impedance

$$Z^*(\omega) = Z' - \mathrm{j}Z'' = R_\mathrm{s} - \frac{\mathrm{j}}{\omega C_\mathrm{s}}$$

complex modulus

$$M^*(\omega) = \frac{1}{\varepsilon^*(\omega)} = M' + \mathrm{j}M'' = \mathrm{j}\omega C_0 Z^*$$

complex admittance

$$Y^* = Y' + \mathrm{j}Y'' = \mathrm{j}\omega C_0 \varepsilon^* = (R_\mathrm{p})^{-1} + \mathrm{j}\omega C_\mathrm{p}$$

complex permittivity $\varepsilon^* = \varepsilon' - \mathrm{j}\varepsilon''$

loss tangent $\tan\delta = \dfrac{\varepsilon''}{\varepsilon'} = -\dfrac{Z'}{Z''} = \dfrac{M''}{M'}$

where $\omega = 2\pi f$ is the angular frequency; C_0 is the geometrical capacitance; and $\mathrm{j}=\sqrt{-1}$. The subscripts "p" and "s" refer to the parallel and series circuit components, respectively.

3.2.1 Impedance analysis

Figure 1 shows the variation of Z' with frequency at different temperatures. It is found that the value of Z' decreases with the increase of both frequency and temperature. The conductivity of materials increases with the rise in temperature and frequency. At high frequency, the value of Z' coincides for all temperatures, implying the possible release of space charge [16].

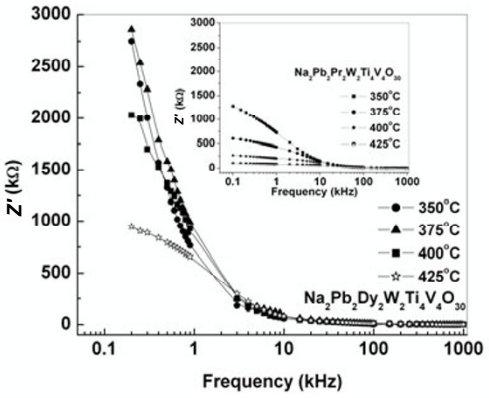

Fig. 1 Variation of Z' with frequency at different temperatures for NPDWTV and NPPWTV.

Figure 2 shows the variation of Z'' with frequency at different temperatures. The value of Z'' becomes

the maximum (Z''_{max}) at higher temperatures. The maximum value of Z'' decreases with the rise in temperature. This exhibits the relaxation in the samples [17]. The increase in the broadening of peak with the rise in temperature suggests the presence of relaxation phenomenon in the materials. The relaxation process occurs due to the presence of immobile species at low temperatures and defects and vacancies at higher temperatures [18,19].

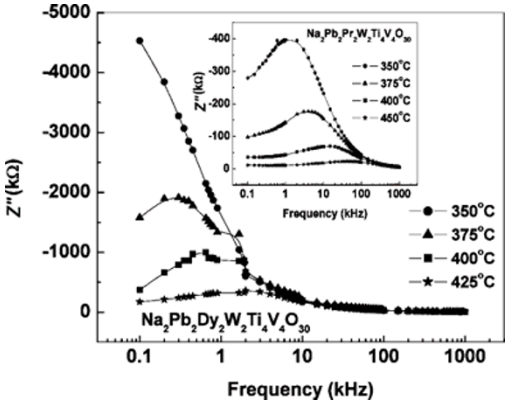

Fig. 2 Variation of Z'' with frequency at different temperatures for NPDWTV and NPPWTV.

Figures 3 and 4 show the variation of Z' with Z'' (Nyquist plot) for a wide frequency range (100 Hz–1 MHz) at different temperatures (325–450 ℃). The depressed or deformed semicircles indicate the presence of non-Debye type of relaxation in the materials. It suggests the presence of a distribution of relaxation time instead of a single relaxation time in the materials [20,21]. The intercept of each semicircle on real Z' axis normally gives the value of bulk resistance. At higher temperatures, there is a tendency to form a second semicircle in one of the samples (NPDWTV). It clearly suggests that this compound has

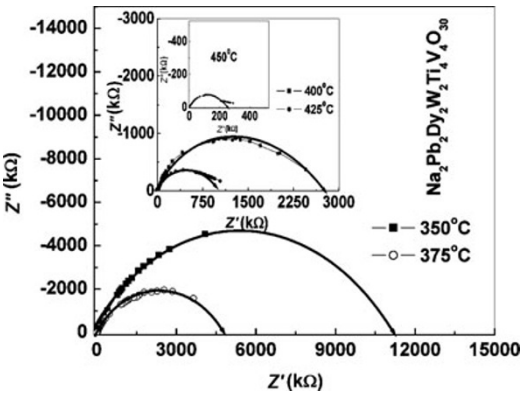

Fig. 3 Variation of Z'' with Z' at different temperatures for NPDWTV.

both grain and grain boundary contributions in impedance.

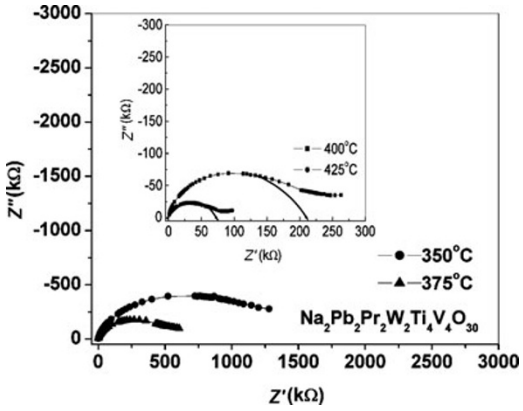

Fig. 4 Variation of Z'' with Z' at different temperatures for NPPWTV.

The semicircles of the impedance spectrum have a characteristic peak occurring at a unique relaxation frequency ($\omega_r = 2\pi f_r$). It can be expressed as

$$\omega_r RC = \omega_r \tau = 1 \quad \text{or} \quad f_r = 1/(2\pi RC)$$

where τ is the relaxation time. The relaxation time due to bulk effect (τ_b) has been calculated using the equation:

$$\omega_r \tau_b = 1 \quad \text{or} \quad \tau_b = 1/(2\pi f_r)$$

Figure 5 shows the variation of $\ln \tau_b$ with the inverse absolute temperature ($10^3/T$). It is observed that the value of τ_b decreases with the rise in temperature for the samples and its temperature dependent characteristics follows Arrhenius relation:

$$\tau_b = \tau_0 \exp(-E_a/k_B T)$$

where τ_0 is the pre-exponential factor; k_B is Boltzmann constant; and T is the absolute temperature. The value of activation energy (E_a) was found to be 1.64 eV and 1.81 eV for NPDWTV and NPPWTV,

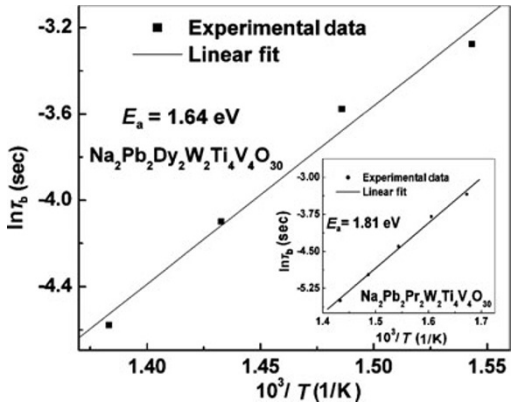

Fig. 5 Variation of relaxation time with temperature for NPDWTV and NPPWTV.

respectively [22].

3.2.2 Modulus analysis

The complex electric modulus formalism can easily distinguish between electrode polarization effect and grain boundary conduction process. It is also useful in detecting the bulk properties as apparent from relaxation time [23,24].

Figure 6 shows the variation of M'' with frequency at different temperatures. It shows that, $M''_{\max}$ shifts towards higher-frequency side with the rise in temperature. This behavior suggests that dielectric relaxation is thermally activated in which the hopping mechanism of charge carriers dominates intrinsically [17]. Asymmetric broadening of the peak indicates the spread of relaxation with different time constants, and hence the relaxation in the materials is considered as non-Debye type [20]. For NPDWTV, two peaks are observed indicating the contribution due to both bulk and grain boundary, because the capacitances of both factors are comparable. The grain boundary effect is not noticed in the impedance plot because the grain boundary resistance is small as compared to the bulk resistance. Impedance spectrum gives more emphasis to elements with the largest resistance whereas modulus spectrum enables to identify the process with the smallest capacitance.

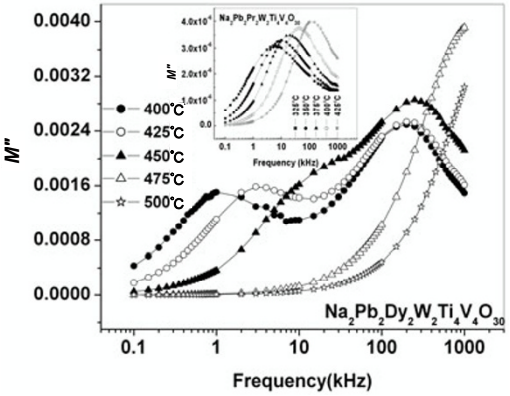

Fig. 6 Variation of M'' with frequency at different temperatures for NPDWTV and NPPWTV.

The scaling behavior of the samples is studied by plotting normalized parameters (i.e., $M''/M''_{\max}$ vs. $\log(f/f_{\max})$), where $f_{\max}$ corresponds to the maximum value of M'', $M''_{\max}$, at different temperatures (Fig. 7). The modulus scaling behavior gives an in-depth knowledge of the dielectric process occurring inside the materials. The low-frequency side of the peak represents a range of frequency in which charge carriers can perform hopping from one site to their neighboring site. The high-frequency side of the peak represents a range of frequency in which charge carriers are spatially confined to their potential well and thus cannot make localized motion inside the well. The small region of the peak represents the transition from long-range mobility to short-range mobility with the increase in frequency [6]. At all the temperatures, the peaks coincide at $\log(f/f_{\max})=1$, which indicates the temperature independent behavior of the relaxation dynamic process occurring in the material [25]. In the case of NPDWTV, two peaks are observed with different time constants, which are due to grain and grain boundary contributions.

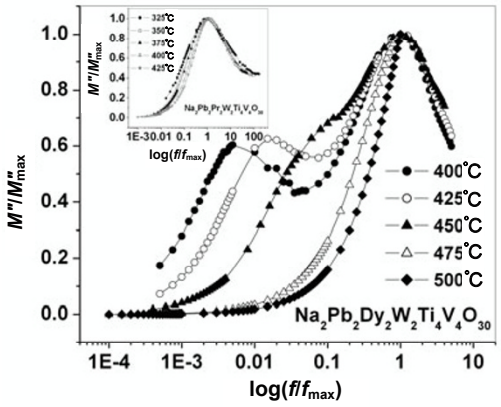

Fig. 7 Plot of $M''/M''_{\max}$ vs. $\log(f/f_{\max})$ at different temperatures for NPDWTV and NPPWTV.

3.3 Electrical conductivity

3.3.1 DC conductivity

The DC conductivity of the samples has been evaluated from the impedance spectrum using a simple relation:

$$\sigma_{\mathrm{DC}}=\frac{t}{R_{\mathrm{b}}A}$$

where t and A represent the thickness and area of the samples, respectively. Figure 8 shows the temperature dependence of DC conductivity. It is observed that σ_{DC} increases with the rise in temperature which supports the negative temperature coefficient of resistance (NTCR) behavior of the samples. The nature of the curve follows Arrhenius relation [20]:

$$\sigma_{\mathrm{DC}}=\sigma_0 \mathrm{e}^{-\frac{E_{\mathrm{a}}}{k_{\mathrm{B}}T}}$$

The activation energy (E_{a}) of NPDWTV in the temperature range of 300–375 ℃ is found to be 0.728 eV, and in the temperature range of 400–475 ℃, it is 1.974 eV. Similarly, E_{a} of NPPWTV in the

temperature range of 225–325 ℃ is 0.441 eV, and in the temperature range of 350–425 ℃, it is 1.113 eV. These values of E_a are different from those calculated from the relaxation time plots. This implies that the charge carriers responsible for conduction and relaxation are different. Besides, the difference in activation energy in low and high temperature range supports the conduction mechanism of hopping type [11].

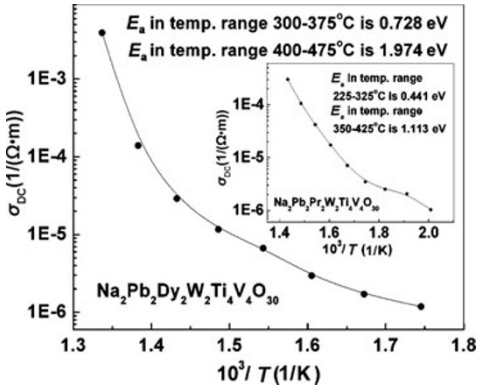

Fig. 8 Variation of DC conductivity with temperature for NPDWTV and NPPWTV.

3.3.2 AC conductivity

The frequency dependence of AC conductivity provides information regarding the nature of charge carriers. The AC electrical conductivity (σ_{AC}) is calculated using an empirical relation:

$$\sigma_{AC} = \omega\varepsilon_r\varepsilon_0 \tan\delta$$

where ε_0 is the permittivity in free space; ω is the angular frequency; and ε_r and $\tan\delta$ are the dielectric parameters. Jonscher made an attempt to explain the behavior of AC conductivity using the following law [26]:

$$\sigma_T(\omega) = \sigma(0) + \sigma_1(\omega) = \sigma_0 + a\omega^n$$

where $\sigma_T(\omega)$ is the total conductivity; $\sigma(0)$ is the frequency independent term giving DC conductivity, and $\sigma_1(\omega)$ is the pure dispersive component of AC conductivity having a characteristic of power law in terms of angular frequency ω and exponent n. The value of exponent n can have a value of $0 \leqslant n \leqslant 1$. This parameter is frequency independent but temperature and material dependent.

Figures 9(a) and 9(b) show the variation of AC conductivity with frequency (usually referred as conductivity spectrum) at different temperatures for NPDWTV and NPPWTV compounds. In these compounds, conductivity curves show dispersion in the low-frequency region. From the nature of graphs, it is obvious that σ_{AC} decreases on the decreasing frequency and becomes nearly independent at low frequency. The extrapolation of the lower frequency gives σ_{DC} . The increasing trend of σ_{AC} with frequency (in the lower-frequency region) may be attributed to the disordering of cations between neighboring-sites and presence of space charge. In the high-frequency region, the curves approach each other for NPPWTV. For NPDWTV, the frequency independent plateau region is observed at higher temperature and higher frequency possibly due to the release of space charge. A close inspection on the conductivity plots reveals that the curves exhibit low-frequency dispersion phenomena obeying Jonscher's power law equation. According to Jonscher [18], the origin of the frequency dependence of conductivity lies in the relaxation phenomena arising due to mobile charge carriers. When a mobile charge hops to a new site from its original position, it remains in a state of displacement between two potential energy minima. Moreover, the conduction behavior of the materials obeys the power law, $\sigma(\omega) \propto \omega^n$, with a slope change governed by n in the low-temperature

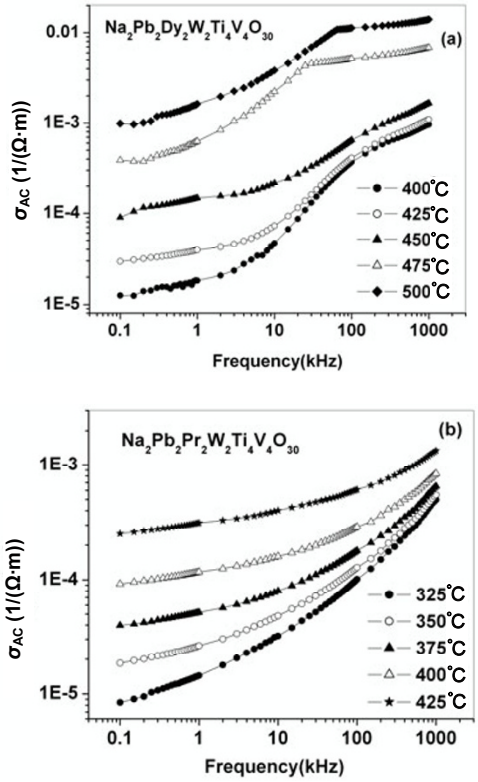

Fig. 9 (a) Variation of AC conductivity with frequency at different temperatures for NPDWTV; (b) variation of AC conductivity with frequency at different temperatures for NPPWTV.

region. According to Funke [27], the value of n has a physical meaning. The value of $n \leqslant 1$ means that the hopping motion involves a translational motion with a sudden hopping, whereas $n > 1$ means that the motion involves localized hopping without the species leaving the neighborhood. The frequency at which slope changes is known as hopping frequency of the polarons (ω_p), and is temperature dependent. The low frequency dispersion has been attributed to the AC conductivity whereas the frequency independent plateau region corresponds to the DC conductivity.

4 Conclusions

The NPDWTV and NPPWTV samples have an orthorhombic TB crystal structures. Detailed studies of electrical properties indicate that the materials exhibit: ① conduction due to the bulk material up to temperature 450 ℃ for both samples; ② electrical transport governed in both the samples at temperature $T > 475$ ℃ characterized by the appearance of two semi-circular arcs in the impedance spectrum; ③ NTCR-type behavior; and ④ temperature-dependent relaxation phenomena. The results of impedance spectrum have been used to estimate the electrical conductivity of the materials. The activation energy estimated from the conducting pattern, relaxation time pattern and modulus pattern are nearly similar. This suggests the presence of similar type of charge carriers in the materials that are responsible for both the electrical conduction and electrical relaxation phenomena in the materials. The activation energy from grain boundary conduction plot suggests the possibility of electrical conduction due to the mobility of the oxide ion. Modulus analysis indicates non-exponential type conductivity relaxation in the material. Comparing the experimental results of NPDWTV and NPPWTV with those of others (as mentioned above), it is suggested that these two materials may be used as good dielectric materials with moderate dielectric permittivity. With the low tangent loss (i.e., high quality factor) in high frequency range, the materials may be used for microwave applications, and also for pyroelectric detector.

References

[1] Singh AK, Choudhary RNP. Study of ferroelectric phase transition in $Pb_3R_3Ti_5Nb_5O_{30}$ (R = rare earth ion) ceramics. *Ferroelectrics* 2005, **325**: 7–14.

[2] Kim MS, Lee JH, Kim JJ, *et al*. Microstructure evolution and dielectric properties of $Ba_{5-x}Na_{2x}Nb_{10}O_{30}$ ceramics with different Ba–Na ratios. *J Solid State Electr* 2006, **10**: 18–23.

[3] Fang L, Zhang H, Huang TH, *et al*. Preparation, structural, and dielectric properties of $Ba_5YZnM_9O_{30}$ (M = Nb, Ta) ceramics. *J Mater Sci* 2005, **40**: 533–535.

[4] Behera B, Nayak P, Choudhary RNP. Structural, dielectric and electrical properties of $NaBa_2X_5O_{15}$ (X = Nb and Ta) ceramics. *Mater Lett* 2005, **59**: 3489–3493.

[5] Hornebecq V, Elissalde C, Reau JM, *et al*. Relaxations in new ferroelectric tantalates with tetragonal tungsten bronze structure. *Ferroelectrics* 2000, **238**: 57–63.

[6] Ganguly P, Jha AK, Deori KL. Complex impedance studies of tungsten–bronze structured $Ba_5SmTi_3Nb_7O_{30}$ ferroelectric ceramics. *Solid State Commun* 2008, **146**: 472–477.

[7] Neurgaonkar RR, Nelson JG, Oliver JR, *et al*. Ferroelectric and structural properties of the tungsten bronze system $K_2Ln^{3+}Nb_5O_{15}$, Ln = La to Lu. *Mater Res Bull* 1990, **25**: 959–970.

[8] Fang L, Zhang H, Yang JF, *et al*. Preparation, characterization and dielectric properties of $Ba_5LnZnTa_9O_{30}$ (Ln = La, Sm) ceramics. *Matet Res Bull* 2004, **39**: 677–682.

[9] Qu YQ, Li AD, Shao QY, *et al*. Structure and electrical properties of strontium barium niobate ceramics. *Mater Res Bull* 2002, **37**: 503–513.

[10] Das PR, Biswal L, Behera B, *et al*. Structural and electrical properties of $Na_2Pb_2Eu_2W_2Ti_4X_4O_{30}$ (X = Nb, Ta) ferroelectric ceramics. *Mater Res Bull* 2009, **44**: 1214–1218.

[11] Das PR, Choudhary RNP, Samantray BK. Diffuse ferroelectric phase transition in $Na_2Pb_2Sm_2W_2Ti_4Nb_4O_{30}$ ceramics. *Mater Chem Phys* 2007, **101**: 228–233.

[12] Das PR, Choudhary RNP, Samantray BK. Diffuse ferroelectric phase transition in $Na_2Pb_2Nd_2W_2Ti_4Nb_4O_{30}$ ceramic. *J Alloys Compd* 2008, **448**: 32–37.

[13] Das PR, Choudhary RNP, Samantray BK. Diffuse phase transition in $Na_2Pb_2R_2W_2Ti_4V_4O_{30}$ (R = Gd, Eu)

ferroelectric ceramics. *J Phys Chem Solids* 2007, **68**: 516–522.

[14] Das PR, Behera B, Choudhary RNP, *et al*. Ferroelectric properties of $Na_2Pb_2R_2W_2Ti_4V_4O_{30}$ (R = Dy, Pr) ceramics. *Res Lett Mater Sci* 2007, Article ID: 91796.

[15] Wu E. POWDMULT—An interactive powder diffraction data interpretation and indexing program, Version 2.5. Bedford Park, Australia: School of Physical Science, Finders University of South Australia.

[16] Plocharski J, Wieczoreck W. PEO based composite solid electrolyte containing nasicon. *Solid State Ionics* 1988, **28–30**: 979–982.

[17] Behera B, Nayak P, Choudhary RNP. Structural and impedance properties of $KBa_2V_5O_{15}$ ceramics. *Mater Res Bull* 2008, **43**: 401–410.

[18] Jonscher AK. The 'universal' dielectric response. *Nature* 1977, **267**: 673–679.

[19] Suman CK, Prasad K, Choudhary RNP. Complex impedance studies on tungsten–bronze electroceramic: $Pb_2Bi_3LaTi_5O_{18}$. *J Mater Sci* 2006, **41**: 369–375.

[20] Sen S, Choudhary RNP, Pramanik P. Structural and electrical properties of Ca^{2+}-modified PZT electroceramics. *Physica B* 2007, **387**: 56–62.

[21] Behera B, Nayak P, Choudhary RNP. Impedance spectroscopy study of $NaBa_2V_5O_{15}$ ceramic. *J Alloys Compd* 2007, **436**: 226–232.

[22] Das PS, Chakraborty PK, Behera B, *et al*. Electrical properties of $Li_2BiV_5O_{15}$ ceramics. *Physica B* 2007, **395**: 98–103.

[23] Sinclair DC, West AR. Impedance and modulus spectroscopy of semiconducting $BaTiO_3$ showing positive temperature coefficient of resistance. *J Appl Phys* 1989, **66**: 3850–3856.

[24] Hodge IM, Ingram MD, West AR. A new method for analysing the a.c. behaviour of polycrystalline solid electrolyte. *J Electroanal Chem Interfacial Electroch* 1975, **58**: 429–432.

[25] Saha S, Sihna TP. Low-temperature scaling behavior of $BaFe_{0.5}Nb_{0.5}O_3$. *Phys Rev B* 2002, **65**: 134103.

[26] Jonscher AK. *Universal Relaxation Law*. London: Chelsea Dielectrics Press, 1996.

[27] Funke K. Jump relaxation in solid electrolytes. *Prog Solid State Ch* 1993, **22**: 111–195.